Published in final edited form as:

Oncogene. 2019 April ; 38(14): 2437–2450. doi:10.1038/s41388-018-0593-5.

Stromal Gas6 promotes the progression of premalignant mammary cells

Angelica M. Gomes[#1], **Emily C. Carron**[#2], **Kylie L. Mills**[1], **Alexa M. Dow**[1], **Zane Gray**[1], **Christopher R. Fecca**[1], **Meredith A. Lakey**[3], **Peter Carmeliet**[4,5,6], **Frances Kittrell**[7], **Daniel Medina**[7], and **Heather L. Machado**[1,‡]

[1]Department of Biochemistry and Molecular Biology, Tulane Cancer Center, Tulane School of Medicine, New Orleans, LA, USA

[2]Division of Cellular Biology, La Jolla Institute for Allergy and Immunology, La Jolla, CA, USA

[3]Ochsner Biorepository, Department of Research, Ochsner Clinic Foundation, New Orleans, LA, USA

[4]Laboratory of Angiogenesis and Vascular Metabolism, Center for Cancer Biology (CCB), Vesalius Research Center, VIB, Leuven, B-3000, Belgium

[5]State Key Laboratory of Ophthalmology, Zhongsan Ophthalmic Center, Sun Yat-Sen University, Guangzhou, China

[6]Laboratory of Angiogenesis and Vascular Metabolism, Department of Oncology and Leuven Cancer Institute (LKI), KU Leuven, Leuven, B-3000, Belgium

[7]Department of Molecular and Cellular Biology, Baylor College of Medicine, Houston, TX, USA

[#] These authors contributed equally to this work.

Abstract

Tumor progression is regulated by a complex interplay between neoplastic cells and the tumor microenvironment. Tumor associated macrophages have been shown to promote breast cancer progression in advanced disease and more recently, in early stage cancers. However, little is known about the macrophage-derived factors that promote tumor progression in early stage lesions. Using a p53-null model of early stage mammary tumor progression, we found that Gas6 is highly expressed in pre-invasive lesions associated with increased infiltrating macrophages, as compared

[‡] Corresponding author: Heather L. Machado, Address: 1430 Tulane Ave, #8543, New Orleans, LA 70112, Phone: 504-988-1753, Fax: 504-988-1024, hmachado@tulane.edu.

Author contributions

A.M.G.: conception and design, collection and assembly of data, data analysis and interpretation, manuscript writing; E.C.C.: conception and design, collection and assembly of data, data analysis and interpretation; K.L.M.: collection and assembly of data; A.M.D.: collection and assembly of data; Z.G.: collection and assembly of data; C.R.F.: collection and assembly of data; M.A.L.: collection and assembly of data; P.C.: collection of data and final approval of manuscript; F.K.: conception, design and final approval of manuscript; D.M.: conception and design, final approval of manuscript; H.L.M.: conception and design, collection and assembly of data, data analysis and interpretation, manuscript writing, financial support.

Conflict of interest

The authors declare no conflicts of interest.

Supplementary information is available at Oncogene's website.

to those with few recruited macrophages. We show that F4/80^{+}CD11b^{+} macrophages produce Gas6 in premalignant lesions *in vivo*, and that macrophage-derived Gas6 induces a tumor-like phenotype *ex vivo*. Using a 3-D co-culture system, we show that macrophage-derived Gas6 activates its receptor Axl and downstream survival signals including Akt and STAT3, which was accompanied by altered E-cadherin expression to induce a malignant morphology. *In vivo* studies demonstrated that deletion of stromal Gas6 delays early stage progression and decreases tumor formation, while tumor growth in established tumors remains unaffected. These studies suggest that macrophage-derived Gas6 is a critical regulator of the transition from premalignant to invasive cancer, and may lead to the development of unique biomarkers of neoplastic progression for patients with early stage breast cancer, including ductal carcinoma *in situ*.

Keywords

Gas6; macrophages; mammary pre-invasive cells; tumor microenvironment

INTRODUCTION

The tumor microenvironment can dictate tissue-specific gene expression, which in turn plays a crucial role in the development of human malignancies (1, 2). Macrophages are differentiated myeloid cells that constitute a major component of the inflammatory infiltrates present in solid tumors. Although macrophages were first thought to contribute to the host response against tumors, it is now well-established that macrophages promote tumor progression and metastasis in a number of cancers, including prostate, bladder, colon and breast (3, 4). In particular, increased macrophages within the tumor microenvironment are associated with poor prognosis in breast cancer patients (5, 6).

Macrophages exhibit enormous plasticity and respond to different stimuli, including cytokines, according to the local environment. Cell responses fall under an umbrella of phenotypes, including activated pro-inflammatory macrophages (often referred to as M1 macrophages), and pro-tumorigenic phenotypes including anti-inflammatory, immunosuppressive, angiogenesis-promoting, invasion-promoting, and others (7, 8). Studies in mouse models have shown that macrophages are recruited to the invasive fronts of established mammary tumors where they exert pro-tumorigenic activities to promote metastasis (9–11). A growing body of literature suggests that macrophages at the pre-invasive stage also have tumor-promoting activities, including immunosuppression and promotion of cell invasion (12, 13). Using a p53-null model of early breast cancer progression, we showed that macrophages are recruited to pre-invasive lesions where they are polarized toward a tumor-promoting phenotype (14). In this model, premalignant cells are serially transplanted into the cleared fat pads of Balb/c mice, where they progress through ductal hyperplasia, low grade mammary intraepithelial neoplasia (MIN), and high grade MIN/invasive tumors at various times post-transplantation (15–17), and thus closely mimic human ductal carcinoma *in situ* (DCIS) progression (17). Gene profiling of pre-invasive lesions revealed that the growth arrest-specific gene 6 (Gas6) is highly expressed in lesions with increased macrophage recruitment and a high tumor-forming potential as

compared to those with few macrophages that rarely form tumors (14), suggesting that Gas6 may regulate premalignant progression.

Gas6 is a vitamin K-dependent cytokine that binds to a family of receptor tyrosine kinases that include Tyro3, Axl and MerTK (TAMR family). Although Gas6 can bind all three receptors, its affinity for Axl is ~100–1000 times higher than MerTK and Tyro3 (18–20). Gas6/TAMR signaling has been shown to regulate proliferation, efferocytosis, leukocyte migration, clearance of apoptotic cells, platelet aggregation, and other biological processes (21–25). In macrophages, Gas6 has emerged as a potent inhibitor of innate immune responses. More recently, Gas6 and Axl have been implicated in the progression of various cancers, sparking interest in targeting this pathway as a potential therapeutic strategy (26, 27). Axl expression has been associated with resistance to EGFR targeted therapy in $EGFR^+$ lung and breast cancers (28, 29), increased metastasis in breast cancers (30, 31), and is correlated with poor overall survival in $Her2^+$ breast cancers (30). However, it is unclear as to whether Gas6/Axl are important during premalignancy. Gas6 was shown to promote prostate cancer cell invasion (32), while Axl-induced breast cancer metastasis was shown to be Gas6-independent (30). Notably, leukocyte-derived Gas6 was shown to promote tumor growth in several different syngeneic tumor models, which was ablated in the presence of $Gas6^{-/-}$ bone marrow-derived macrophages (33). The potential role of Gas6 and TAMRs in localized invasion during the switch from premalignant to invasive breast cancer has not been studied.

In this study, we explore whether Gas6 signaling mediates early breast cancer progression. We show that Gas6 was highly expressed in pre-invasive lesions, but declined in invasive tumors, suggesting that this cytokine may be important for the transition from pre-invasive to invasive cancer. Using a 3-D co-culture *ex vivo* system, we demonstrate that macrophage-derived Gas6 promotes a tumor-like phenotype in premalignant cells and activates Axl, Akt and STAT3 to induce cell survival, which is accompanied by mislocalization of E-cadherin. Finally, we show that stromal Gas6 promotes primary tumor formation *in vivo*. These studies have critical implications for targeting macrophages and Gas6/Axl signaling in early stage breast cancer.

RESULTS

Gas6 and TAMR expression in pre-invasive lesions.

Using a p53-null transplantable syngeneic model of early progression, we previously showed that macrophages are recruited to pre-invasive lesions with a high tumor-forming potential (PN1a) as compared to those that rarely form tumors (PN1b). Gene profiling showed that Gas6 was upregulated ~10 fold in PN1a lesions as compared to PN1b lesions, and ~30 fold as compared to $p53^{-/-}$ mammary glands (14). To confirm these results, we performed an ELISA for Gas6 on whole cell lysates that were harvested from mammary glands containing transplanted PN1a and PN1b tissue at various stages of progression. Mammary glands from wildtype and $p53^{-/-}$ mice were also evaluated as controls (Figure 1a). While Gas6 levels were nearly undetectable in PN1b lesions, Gas6 was highly expressed in PN1a lesions at 8 and 16 weeks post-transplantation and declined in established tumors. Immunostaining for Gas6 showed strong expression in PN1a lesions in both

epithelial and stromal compartments, which was decreased in PN1b lesions. In support of the ELISA, Gas6 expression was decreased in PN1a tumors as compared to pre-invasive lesions (Figure 1b). We also examined Gas6 expression in the well-characterized C3(1)TAg mouse model in which low grade MIN develop by 8 weeks of age, progress to high grade MIN by 12 weeks, and invasive cancer by 16 weeks or later. Similar to the PN1a lesions, Gas6 was highly expressed in early C3(1)TAg MIN (Supplemental Figure 1a). To determine which cell type was secreting Gas6 in PN1a lesions, we FACS-sorted macrophages ($CD45^+CD11b^+F480^+$), T-cells ($CD45^+CD3^+CD11b^-$), and $CD45^-$ cells (primarily containing epithelial cells) and performed qPCR. Figure 1c shows that Gas6 expression was highest in $CD45^+$ cells as compared to $CD45^-$ cells, with increased expression in macrophages (Figure 1c and Supplemental Figure 1b). Next, we examined Gas6 and receptor expression in LIN^--sorted cells (epithelial cells) from normal mammary glands and premalignant lesions. Gas6 and Axl were highly expressed in PN1a epithelium while expression was significantly lower in MECs and PN1b epithelium (Figure 1d). While MerTK was expressed in all cell types analyzed, Tyro3 was barely detectable by qPCR (data not shown). To determine the clinical relevance of these results, we analyzed 23 patient samples of pre-invasive ductal carcinoma *in situ* (DCIS), the non-obligatory precursor of invasive carcinoma (Supplemental Table 1). While epithelial Gas6 was variable (65% low, staining 35% high), 86% of the DCIS samples showed stromal staining for Gas6, including cells with cytological features of macrophages (Figure 1e). Gas6 and CD68 co-localized, suggesting that stromal Gas6 expression included macrophages (Figure 1f). These results suggest that Gas6 signaling may regulate human DCIS progression.

Macrophage-derived Gas6 induces a malignant phenotype in pre-invasive mammary cells.

We previously showed that PN1a cells polarize bone marrow-derived macrophages (BMDMs) to a tumor-promoting phenotype, and induce Gas6 expression in BMDMs (14). Using a 3-D co-culture system, we showed that BMDMs induce the formation of tumor-like structures in primary PN1a cells *ex vivo* (14). Therefore, we next asked whether this macrophage-mediated phenotype is dependent on Gas6. Epithelial cells were isolated from PN1a lesions and cultured in Matrigel as previously described (34), where round, organized structures developed, characterized by luminal cytokeratin (CK) 8 and basal CK14 expression. After three days of culture, BMDMs isolated from wildtype or $Gas6^{-/-}$ mice were added to the cultures and grown for an additional 10 days. As expected, co-culture with wildtype BMDMs induced a tumor-like phenotype as compared to PN1a alone, characterized by irregular, disorganized structures with disrupted integrin α6 (basal polarity marker) expression and increased CK14 expression (Figure 2a). In contrast, co-culture with $Gas6^{-/-}$ BMDMs resulted in primarily non-malignant structures indistinguishable from colonies formed by PN1a cells alone, with an intact basal layer marked by integrin α6 staining and CK14 expression. Quantification of non-malignant and tumor-like colonies showed a significant decrease in malignant structures in co-cultures with $Gas6^{-/-}$ BMDMs as compared to wildtype BMDMs (Figure 2b). Since both macrophages and PN1a cells express Gas6 (Figure 1b,c), we asked whether secreted Gas6 was indeed decreased in cells co-cultured with $Gas6^{-/-}$ BMDMs. PN1a cells alone and with $Gas6^{-/-}$ BMDMs expressed low levels of Gas6 as compared to those cultured with wildtype BMDMs (Figure 2c), suggesting that PN1a cells produced negligible levels of Gas6. Notably, wildtype BMDMs

alone secreted nearly undetectable levels of Gas6, supporting our previous results showing that PN1a cells induce Gas6 expression in macrophages (14). These results suggest that macrophage-derived Gas6 promotes a malignant phenotype *in vitro*.

We previously showed that primary PN1a conditioned media induced the expression of Gas6 as well as a number of tumor-promoting cytokines in macrophages, suggesting that PN1a cells polarize macrophages toward a pro-tumorigenic phenotype. Thus, it is possible that the malignant phenotype observed in co-cultures is due to the presence of tumor-polarized macrophages, independent of Gas6. To test whether Gas6 is required for macrophage polarization, we exposed wildtype or $Gas6^{-/-}$ BMDMs to PN1a conditioned media and analyzed gene expression of *Vegfa*, *Tnfa*, *Arg1*, *Il6*, and *Il10*. Surprisingly, PN1a cells induced similar levels of pro-tumor genes in both wildtype and $Gas6^{-/-}$ BMDMs, suggesting that Gas6 is not required for polarization (Supplemental Figure 2). To determine whether Gas6 alone is sufficient to induce a tumor-like phenotype, we treated primary PN1a cells with various concentrations of recombinant Gas6 (rGas6) and analyzed their morphology. Figure 3 shows a significant increase in tumor-like colonies in Gas6-treated cells as compared to vehicle-treated, mimicking PN1a cells that were co-cultured with wildtype BMDMs (Figure 3a,b). Altered integrin α6 localization and increased pAxl expression was observed in Gas6-treated cells as compared to controls. Quantification of tumor-like colonies showed a significant increase in $pAxl^{+}$ cells as compared to $pAxl^{-}$ cells in malignant structures, suggesting a link between activated Axl and the malignant phenotype (Figure 3c). To validate these findings, primary cells from 16 week C3(1)TAg lesions were cultured in 3-D in the presence or absence of exogenous Gas6, or wildtype or $Gas6^{-/-}$ BMDMs. Gas6 treatment induced a tumor-like phenotype exemplified by invasive $CK14^{+}$ positive cells (Supplemental Figure 3a). Similar to the PN1a model, wildtype BMDMs induced a tumor-like phenotype, while co-culture with $Gas6^{-/-}$ BMDMs resulted in non-malignant colonies (Supplemental Figure 3b). Together, these results suggest that macrophages induce the formation of tumor-like colonies in pre-invasive cells in a Gas6-dependent manner.

PN1a cells are pre-invasive and have a high tumor-forming potential. To determine whether Gas6 alone can induce changes in normal cells, normal mouse mammary epithelial cells (MECs) were cultured in 3-D in the presence or absence of rGas6 and structures were analyzed. There was no observed difference in morphology, size, or polarity, although there was a modest increase in the number of colonies formed (Supplemental Figure 4a and data not shown). To address whether Gas6/Axl was sufficient to induce malignant changes in non-invasive premalignant cells, a $p53^{-/-}$ cell line (PN2cl) was. These cells were originally derived from primary PN2 outgrowths, which express low levels of Axl (Supplemental Figure 4b) and have a low tumor-forming potential (35). Axl was overexpressed in PN2cl (pLeGO-iG empty vector control or pLeGO-iG-Axl), treated with or without rGas6 in 3-D culture, and the phenotype was assessed. All PN2cl colonies resembled organized, non-malignant structures, suggesting that Gas6/Axl is not sufficient to induce a tumor-like phenotype in non-invasive cells, although there was a significant increase in colony size of Gas6-treated cells (Supplemental Figure 4b). These results suggest that although Gas6 may regulate growth in non-invasive cells, it is likely not an oncogenic driver during cancer initiation.

Gas6 activates Axl in premalignant cells to induce pro-survival signals.

Given that Gas6 is a ligand for the TAMR family, and our premalignant cells expressed both Axl and MerTK (Figure 1), we analyzed whether co-culture with BMDMs activated both receptors. pAxl was expressed basally in PN1a cells cultured alone, whereas PN1a cells co-cultured with wildtype BMDMs showed pAxl expression throughout the tumor-like structures (Figure 4a), similar to that observed when cells were treated with rGas6. In contrast, pAxl expression was basally-restricted in Gas6$^{-/-}$ BMDM co-cultured PN1a cells, consistent with the observed non-malignant phenotype. Under all conditions, pMerTK was undetectable in PN1a cells, although pMerTK was expressed in BMDMs present in our co-culture system (Figure 4b). These data suggest that macrophage-derived Gas6 preferentially activates Axl signaling in premalignant cells.

To further characterize the tumor-like phenotypes observed, we stained co-cultures with antibodies to detect proliferation (Ki-67) and apoptosis [cleaved caspase 3 (CC3)], since Gas6/Axl signaling has been shown to regulate these processes (36, 37). Figure 5 shows that CC3 expression was significantly decreased by 50% in PN1a cells co-cultured with wildtype BMDMs as compared to Gas6$^{-/-}$ BMDMs or PN1a alone (Figure 5a). A modest increase in proliferation was observed in cells co-cultured with wildtype BMDMs as compared to other conditions, however this increase was not statistically significant (Figure 5b). These results suggest that Gas6 protects PN1a cells from apoptosis.

Gas6/Axl signal transduction has previously been shown to induce anti-apoptotic effects during tumor progression by activating a number of pathways, including AKT, STAT3, and NFκB [reviewed in (38)]. Therefore, we next addressed whether these pathways were altered in the 3-D co-culture model. pAKT expression was significantly increased in PN1a cells co-cultured with wildtype BMDMs as compared to Gas6$^{-/-}$ BMDMs (Figure 6a). Similarly, pSTAT3 was barely detectable in Gas6$^{-/-}$ BMDM co-cultures, but significantly increased in malignant structures formed in wildtype BMDM co-cultures (Figure 6b). In contrast, there was no difference in nuclear localization or expression of NF-κB (p65/p105) (Supplemental Figure 5). Since Axl activation has been implicated as both an upstream and downstream regulator of the epithelial mesenchymal transition (EMT) during tumor metastasis (31, 39), we analyzed E-cadherin expression in PN lesions *in vivo*. E-cadherin was uniformly expressed in pre-invasive PN1a and PN1b lesions, however by 18 weeks, expression was reduced in PN1a lesions (Figure 7a). In support, PN1a cells co-cultured with wildtype BMDMs showed mislocalized E-cadherin staining and decreased expression as compared to PN1a cells cultured alone or with Gas6$^{-/-}$ BMDMs (Figure 7b). Collectively, these results suggest that macrophage-derived Gas6 promotes the survival of pre-invasive cells in a paracrine fashion, possibly by activating pAKT and pSTAT3, and may induce EMT changes in pre-invasive cells.

Deletion of stromal-Gas6 delays progression to invasive cancer *in vivo*.

Our *in vitro* data show that Gas6/Axl signaling is critical for malignant changes in pre-invasive cells, suggesting that macrophage-derived Gas6 mediates early stage breast cancer progression. To test whether stromal Gas6 has tumor-promoting activity in pre-invasive stages of mammary tumorigenesis, we performed *in vivo* studies using two cohorts of

animals. PN1a cells were injected into the cleared fat pads of wildtype or Gas6$^{-/-}$ mice, and mammary glands were analyzed at early and late stages of progression. In cohort 1, mice were euthanized at 6 weeks post-transplantation, where lesions resemble simple ductal hyperplasia to low grade MIN (14). Whole mount analysis showed that there was no difference in the percent of fat pad filled in wildtype and Gas6$^{-/-}$ mice, suggesting that Gas6 is not required for ductal outgrowth (Supplemental Figure 6a). The majority of the lesions showed simple ductal hyperplasia, indicating that both groups of lesions were in the earliest stage of progression (Supplemental Figure 6b). Quantification of Ki-67^{+} epithelial cells showed a significant decrease in proliferation in PN1a lesions from Gas6$^{-/-}$ mice as compared to wildtype (Supplemental Figure 6c). In support of our *in vitro* results, STAT3 activation in PN1a lesions was higher in wild type mice as compared to Gas6$^{-/-}$ mice (Supplemental Figure 6d). Finally, CC3 staining revealed a modest increase in apoptosis in PN1a lesions from Gas6$^{-/-}$ mice as compared to wildtype (Supplemental Figure 6e). However, at this early stage of progression, apoptosis is not a predominant event as compared to late stages, which may account for the small difference observed between the groups.

In a second cohort of mice, we addressed whether Gas6 deletion affected palpable tumor formation and growth. Tumor growth was determined by measuring tumors every other day until they reached 1 cm in diameter, at which time the mice were euthanized. A Kaplan-Meier curve shows that there was a significant increase in the onset of measurable tumors in wildtype as compared to Gas6$^{-/-}$ mice, indicating that there was a delay in progression to invasive tumors in Gas6$^{-/-}$ mice (Figure 8a). Similarly, there was a significant increase in the time that tumors reached 1 cm in diameter in wildtype mice as compared to Gas6$^{-/-}$ mice (Figure 8b). Interestingly, there was no significant difference in tumor growth between wildtype and Gas6$^{-/-}$ mice, suggesting that once tumors formed, Gas6 is not required for tumor progression (Figure 8c). Quantification of F4/80^{+} cells showed no difference in macrophage number in tumors from wildtype and Gas6$^{-/-}$ mice (Supplemental Figure 7). Collectively, these data suggest that stromal Gas6 promotes the transition to invasive cancer in early stage mammary lesions.

DISCUSSION

There has been tremendous interest in targeting the tumor microenvironment, and particularly macrophages, as a therapeutic strategy for metastatic breast cancer. It is well-established that macrophages play an instrumental role in promoting the progression of established tumors, by secreting a number of factors that induce angiogenesis and cellular invasion. Although macrophages were previously believed to exert a pro-inflammatory, anti-tumor role in early stage lesions, a growing body of literature suggests that macrophages at the pre-invasive stage also have tumor-promoting functions, including immunosuppression and promotion of cell invasion (12, 13, 40). Using a p53-null syngeneic mouse model of early stage progression, we previously showed that macrophages are recruited to premalignant lesions with a high tumor-forming potential, but were limited in lesions that do not progress to invasive cancer. Macrophage ablation at the pre-invasive stage caused a significant delay in early progression, decreased localized invasion, and a significant reduction in tumor formation (14). In the present study, we identified Gas6 as an important

macrophage factor that is induced by premalignant cells upon macrophage infiltration into ductal hyperplasias (Figure 1). Using a 3-D *ex vivo* co-culture system, we showed that macrophages induce a tumor-like phenotype in premalignant cells in a Gas6-dependent manner, activating the Axl receptor, inducing cell survival and regulating E-cadherin expression (Figures 2–7). Others have shown that leukocyte-derived Gas6 promotes tumor growth of numerous cancer cell lines, including 4T1 cells, *in vivo* (33). However, these models are highly aggressive and do not progress through distinct stages of premalignancy, thus it remained unclear as to whether Gas6/Axl regulate DCIS progression. Our studies utilizing an established mouse model of MIN progression (41) showed that deletion of stromal Gas6 *in vivo* delayed tumor formation, but had no effect on tumor growth once primary tumors were established (Figure 8). These results suggest that stromal Gas6, potentially macrophage-derived, regulates the transition from pre-invasive to invasive cancer.

Gas6/Axl signaling has been shown to promote survival, proliferation and invasion of cancer cells *in vitro* and *in vivo*. Gas6 has the highest affinity for Axl, which can be activated by both ligand-dependent and -independent mechanisms. Our *in vitro* data showed that Axl was preferentially activated by macrophages in a Gas6-dependent manner, with consequent AKT and STAT3 activation, and increased cell survival (Figures 3–6). In support, others have shown Gas6/Axl induced cell survival by activating P13K/AKT, downregulating Bad and increasing Bcl2 (42, 43). More recently, using the MMTV-Neu mouse mammary tumor model, Goyette *et al* demonstrated increased apoptosis in $Neu^{+}Gas6^{-/-}$ tumors as compared to $Neu^{+}Gas6^{+/+}$ (30). Interestingly, PN1a cells cultured alone or with $Gas6^{-/-}$ BMDMs displayed basally localized pAxl expression (Figure 4). It is possible that other receptor tyrosine kinases such as HER2 or EGFR, which have been shown to activate Axl in a ligand-independent fashion (30, 44), induced pAxl in our system. Alternatively, autocrine Gas6 signaling may be activating Axl, as low levels of Gas6 were detected (Figure 2c). However, these mechanisms are unlikely to contribute to cell survival in our pre-invasive cells since pAKT and pSTAT3 were significantly decreased, while CC3 was significantly increased, in the observed non-malignant structures in PN1a cells cultured alone or with $Gas6^{-/-}$ BMDMs. It is well established that Gas6/Axl signaling induces acquisition of EMT features required for invasion in several tumor mouse models of metastasis (30, 31, 39). In support of this concept, our data showed that macrophage-derived Gas6 regulates E-cadherin localization and expression, suggesting that it may modulate the EMT program.

Several studies have correlated Gas6/TAMR expression with poor prognosis in different cancers. High Gas6 expression in ovarian cancer (45), glioblastoma (46), and non-small cell lung cancer (NSCLC) (46) was shown to predict poor overall survival. Similarly, Axl expression has been correlated with poor outcome in acute myeloid leukemia (47), metastatic renal cell carcinoma (48), and several other cancers, and was shown to contribute to resistance to EGFR-targeted therapies in NSCLC (28). In breast cancer, numerous studies have suggested that Axl is an important negative prognostic factor in triple-negative and $Her2^{+}$ metastatic breast cancer (30, 49). However, it is unclear as to whether Axl is activated by Gas6 during metastasis. Gas6 mRNA expression was shown to correlate with progesterone receptor B (PRB) in a panel of 49 breast carcinomas, and was associated with favorable prognostic parameters including lymph node negativity, low nuclear morphology, and smaller tumor size (50). Additionally, it was recently shown in a mouse model of $Her2^{+}$

breast cancer that Axl, but not Gas6, is required for the metastasis of established tumors (30). Interestingly, we showed that Gas6 expression increased in pre-invasive hyperplastic lesions as compared to the normal mammary gland, but decreased in invasive tumors as compared to pre-invasive lesions (Figure 1), even though macrophages continue to increase (14). Furthermore, our *in vivo* studies showed that once tumors were established, growth was not altered by Gas6 deletion (Figure 8). These results suggest that Gas6 signaling may be shut down after the transition to invasive cancer, and thus primarily functions during premalignancy.

Inhibition of Axl phosphorylation is a basis for cancer therapeutic modalities that are under development, and more than 17 Axl inhibitors are currently in preclinical or clinical trials (51). Efforts have also been made to inhibit the interaction between Gas6 and Axl with an Axl decoy recptor, MYD1–72, which has high affinity for Gas6, and effectively blocks Gas6 signaling. This drug has been shown to decrease metastasis of human ovarian cancer cells and to blunt tumor growth and metastasis of mouse mammary tumor cells (27). Additionally, warfarin, a vitamin K antagonist, inhibits Gas6-mediated Axl activation and as a consequence, decreases proliferation, invasion and metastasis of pancreatic tumor cells (52). Our studies suggest that stromal Gas6, and potentially macrophage Gas6, regulates the pre-invasive to invasive transition in a mouse model of premalignant progression. These studies have critical implications for dual targeting the stroma and pre-invasive epithelium with Gas6/Axl inhibitors as a potential prevention or treatment strategy of human DCIS.

MATERIALS AND METHODS

Animal Models

Mice were maintained in a pathogen-free facility under the NIH Guide for the Care and Use of Experimental Animals with approval from the Tulane School of Medicine Institutional Animal Care and Use Committee. BALB/cAnHsd (Balb/c) mice were obtained from Envigo, C57BL/6J mice were obtained from the The Jackson Laboratory, and C3(1)Tag mice (FVB/NJ) were obtained from the University of North Carolina School of Medicine Mouse Phase 1 Unit (Chapel Hill, NC). *Trp53*$^{-/-}$ mice have been described (53) and are maintained in the Balb/c strain. *Gas6*$^{-/-}$ mice were maintained and genotyped as previously described (22) and were backcrossed eight generations to the Balb/c strain. Experiments were performed using either C57BL/6J or Balb/c strains. *Trp53*$^{-/-}$ outgrowth lines PN1a and PN1b were maintained by serial transplantation into the cleared fat pads (#4 contralateral mammary glands) of 3-week-old female Balb/c mice as previously described (17).

ELISA

The Mouse Gas6 Quantikine® ELISA kit (R&D Systems, Minneapolis, MN, US) was used according to the manufacturer's instructions. Details are described in Supplemental Methods.

FACS analysis

Fluorescence activated cell sorting (FACS) was performed as previously described (14). Details are described in Supplemental Methods.

RNA isolation and qPCR

RNA isolation and qPCR was performed as described in the Supplemental Methods.

Clinical samples

Twenty three formalin fixed human DCIS samples were obtained from 3 sources: Louisiana Cancer Research Consortium Biospecimen Core (New Orleans, LA), the Biorepository Unit at Ochsner Medical Center (New Orleans, LA), and the NCI Cooperative Human Tissue Network (University of Virginia School of Medicine, VA). DCIS patient samples are described in Supplemental Table 1. Immunostaining using antibodies to Gas6 and CD68 (Supplemental Table 2) was performed as previously described (14), where tissues were blocked with 5%BSA/PBST. Images were acquired using a Nikon Eclipse microscope.

Immunohistochemistry

Paraffin-embedded tissues were processed and stained with various antibodies (Supplemental Table 2) as previously described (14). Details and modifications are described in Supplemental Methods.

Three-dimensional co-culture

Bone marrow cells from the femurs and tibias of adult C57BL/6J mice were isolated and differentiated into BMDMs as previously described (14, 54, 55). Epithelial cells were isolated from mammary glands containing PN1a 8-week outgrowths as described (14). PN1a cells and PKH26-labeled (Sigma Aldrich) BMDMs were co-cultured on growth factor-reduced Matrigel® (BD Bioscience) as described (14). For treatment with recombinant Gas6 (rGas6), mouse rGas6 (R&D Systems) or PBS (vehicle control) were added to the cultures on day 3, and incubated at 37°C for an additional 10 days, replacing the media/rGas6 every 3 days. Phase contrast images were obtained using an Evos FL microscope (Thermo Fisher Scientific, Waltham, MA, USA). For quantification of the number of non-malignant and tumor-like colonies, at least 30 structures per group were analyzed (n=3). Immunostaining was performed as previously described (14) and antibodies are listed in Supplemental Table 2. Confocal images were acquired under a 60X objective using a Nikon A1plus confocal microscope.

In vivo studies

For analysis of tumor progression *in vivo*, PN1a cells were isolated as described above, and 1000 cells/10μl in a 1:1 solution of PBS:growth factor-reduced Matrigel® were injected into the cleared fat pads (#4 contralateral) of 3–6-week-old wildtype or $Gas6^{-/-}$ balb/c mice using a 26G needle and a 50μl Hamilton syringe. Cells were injected into both contralateral mammary glands and allowed to grow for 6 weeks. For the tumor study, cells were injected into one mammary gland/animal and allowed to grow for the indicated times. Once palpable, tumor size was measured every other day and mice were euthanized when tumors reached 1cm in diameter. For whole mounts, glands were fixed in cold 4% paraformaldehyde for 2 hours, incubated with acetone for 1 hour at room temperature to remove the fat, and stained with a 50% glycerol/PBS solution containing 10ug/mL DAPI overnight. Mammary glands

were washed with 50% glycerol/PBS, imaged on a Leica M165 FC stereoscope (Leica Biosystems), and subsequently embedded in paraffin.

Statistical analysis

All statistical analyses were performed using GraphPad Prism 6/7. Fold change significance for qPCR was calculated using a two-way ANOVA (Figure 1) or an unpaired t-test (Supplemental Figure 2). For 3-D co-culture experiments, the significance of the number of non-malignant and tumor-like acini was calculated using a contingency table and Chi-squared analysis. For quantification of Ki67, CC3, pAKT, and pSTAT3 from *in vitro* experiments and ELISA, the significance was calculated using a one-way ANOVA. For pSTAT3, Ki67 and CC3 from the *in vivo* experiments the significance was calculated using an unpaired t-test. For the Kaplan-Meier curve the log rank test was used. For the tumor growth analysis and time of sacrifice an unpaired t-test was used.

Supplementary Material

Refer to Web version on PubMed Central for supplementary material.

Acknowledgements

This work was supported by Susan G. Komen CCR16377665 (H.L.M), NIH R01 CA212518 (H.L.M.), and the Tulane Cancer Center through the Cancer Crusaders of New Orleans. We would like to thank Dr. Dorota Wyczechowska from the LCRC Cell Immunology and Metabolism Core (NIH/NIGMS 1P30GM114732–01) for assistance with FACS and Dr. Leann Myers for help with statistical analysis. We would like to acknowledge Alexandra Giardina at the LCRC Biospecimen Core and Dr. Lyndsey Buckner Baiamonte, Jeannine Ascani, and Dr. Michelle Ponder at the Oschner Biorepository Unit for human DCIS tissues.

REFERENCES

1. Levental KR, Yu H, Kass L, Lakins JN, Egeblad M, Erler JT, et al. Matrix crosslinking forces tumor progression by enhancing integrin signaling. Cell. 2009;139(5):891–906. [PubMed: 19931152]
2. Lyons TR, O'Brien J, Borges VF, Conklin MW, Keely PJ, Eliceiri KW, et al. Postpartum mammary gland involution drives progression of ductal carcinoma in situ through collagen and COX-2. Nat Med. 2011;17(9):1109–15. [PubMed: 21822285]
3. Bingle L, Brown NJ, Lewis CE. The role of tumour-associated macrophages in tumour progression: implications for new anticancer therapies. J Pathol. 2002;196(3):254–65. [PubMed: 11857487]
4. Qian BZ, Pollard JW. Macrophage diversity enhances tumor progression and metastasis. Cell. 2010;141(1):39–51. [PubMed: 20371344]
5. Qian BZ, Li J, Zhang H, Kitamura T, Zhang J, Campion LR, et al. CCL2 recruits inflammatory monocytes to facilitate breast-tumour metastasis. Nature. 2011;475(7355):222–5. [PubMed: 21654748]
6. Medrek C, Ponten F, Jirstrom K, Leandersson K. The presence of tumor associated macrophages in tumor stroma as a prognostic marker for breast cancer patients. BMC Cancer. 2012;12:306. [PubMed: 22824040]
7. Xue J, Schmidt SV, Sander J, Draffehn A, Krebs W, Quester I, et al. Transcriptome-based network analysis reveals a spectrum model of human macrophage activation. Immunity. 2014;40(2):274–88. [PubMed: 24530056]
8. Noy R, Pollard JW. Tumor-associated macrophages: from mechanisms to therapy. Immunity. 2014;41(1):49–61. [PubMed: 25035953]
9. Gocheva V, Wang HW, Gadea BB, Shree T, Hunter KE, Garfall AL, et al. IL-4 induces cathepsin protease activity in tumor-associated macrophages to promote cancer growth and invasion. Genes Dev. 2010;24(3):241–55. [PubMed: 20080943]

10. Lin EY, Pollard JW. Macrophages: modulators of breast cancer progression. Novartis Found Symp. 2004;256:158–68; discussion 68–72, 259–69. [PubMed: 15027489]
11. Lin EY, Li JF, Gnatovskiy L, Deng Y, Zhu L, Grzesik DA, et al. Macrophages regulate the angiogenic switch in a mouse model of breast cancer. Cancer Res. 2006;66(23):11238–46. [PubMed: 17114237]
12. Bohrer LR, Schwertfeger KL. Macrophages promote fibroblast growth factor receptor-driven tumor cell migration and invasion in a CXCR2-dependent manner. Mol Cancer Res. 2012;10(10): 1294–305. [PubMed: 22893608]
13. Wang W, Li X, Zheng D, Zhang D, Peng X, Zhang X, et al. Dynamic changes and functions of macrophages and M1/M2 subpopulations during ulcerative colitis-associated carcinogenesis in an AOM/DSS mouse model. Mol Med Rep. 2015;11(4):2397–406. [PubMed: 25434400]
14. Carron EC, Homra S, Rosenberg J, Coffelt SB, Kittrell F, Zhang Y, et al. Macrophages promote the progression of premalignant mammary lesions to invasive cancer. Oncotarget. 2017;8(31):50731–46. [PubMed: 28881599]
15. Jerry DJ, Kittrell FS, Kuperwasser C, Laucirica R, Dickinson ES, Bonilla PJ, et al. A mammary-specific model demonstrates the role of the p53 tumor suppressor gene in tumor development. Oncogene. 2000;19(8):1052–8. [PubMed: 10713689]
16. Medina D, Kittrell FS, Hill J, Shepard A, Thordarson G, Brown P. Tamoxifen inhibition of estrogen receptor-alpha-negative mouse mammary tumorigenesis. Cancer Res. 2005;65(8):3493–6. [PubMed: 15833886]
17. Medina D, Kittrell FS, Shepard A, Stephens LC, Jiang C, Lu J, et al. Biological and genetic properties of the p53 null preneoplastic mammary epithelium. FASEB J. 2002;16(8):881–3. [PubMed: 11967232]
18. Tsou WI, Nguyen KQ, Calarese DA, Garforth SJ, Antes AL, Smirnov SV, et al. Receptor tyrosine kinases, TYRO3, AXL, and MER, demonstrate distinct patterns and complex regulation of ligand-induced activation. J Biol Chem. 2014;289(37):25750–63. [PubMed: 25074926]
19. Lew ED, Oh J, Burrola PG, Lax I, Zagórska A, Través PG, et al. Differential TAM receptor-ligand-phospholipid interactions delimit differential TAM bioactivities. Elife. 2014;3.
20. Geng K, Kumar S, Kimani SG, Kholodovych V, Kasikara C, Mizuno K, et al. Requirement of Gamma-Carboxyglutamic Acid Modification and Phosphatidylserine Binding for the Activation of Tyro3, Axl, and Mertk Receptors by Growth Arrest-Specific 6. Front Immunol. 2017;8:1521. [PubMed: 29176978]
21. Tjwa M, Bellido-Martin L, Lin Y, Lutgens E, Plaisance S, Bono F, et al. Gas6 promotes inflammation by enhancing interactions between endothelial cells, platelets, and leukocytes. Blood. 2008;111(8):4096–105. [PubMed: 18156494]
22. Angelillo-Scherrer A, de Frutos P, Aparicio C, Melis E, Savi P, Lupu F, et al. Deficiency or inhibition of Gas6 causes platelet dysfunction and protects mice against thrombosis. Nat Med. 2001;7(2):215–21. [PubMed: 11175853]
23. Ishimoto Y, Ohashi K, Mizuno K, Nakano T. Promotion of the uptake of PS liposomes and apoptotic cells by a product of growth arrest-specific gene, gas6. J Biochem. 2000;127(3):411–7. [PubMed: 10731712]
24. Yanagita M, Arai H, Nakano T, Ohashi K, Mizuno K, Fukatsu A, et al. Gas6 induces mesangial cell proliferation via latent transcription factor STAT3. J Biol Chem. 2001;276(45):42364–9. [PubMed: 11546821]
25. Wu G, Ma Z, Hu W, Wang D, Gong B, Fan C, et al. Molecular insights of Gas6/TAM in cancer development and therapy. Cell Death Dis. 2017;8(3):e2700. [PubMed: 28333143]
26. Holland SJ, Pan A, Franci C, Hu Y, Chang B, Li W, et al. R428, a selective small molecule inhibitor of Axl kinase, blocks tumor spread and prolongs survival in models of metastatic breast cancer. Cancer Res. 2010;70(4):1544–54. [PubMed: 20145120]
27. Kariolis MS, Miao YR, Diep A, Nash SE, Olcina MM, Jiang D, et al. Inhibition of the GAS6/AXL pathway augments the efficacy of chemotherapies. J Clin Invest. 2017;127(1):183–98. [PubMed: 27893463]

28. Zhang Z, Lee JC, Lin L, Olivas V, Au V, LaFramboise T, et al. Activation of the AXL kinase causes resistance to EGFR-targeted therapy in lung cancer. Nat Genet. 2012;44(8):852–60. [PubMed: 22751098]
29. Meyer AS, Miller MA, Gertler FB, Lauffenburger DA. The receptor AXL diversifies EGFR signaling and limits the response to EGFR-targeted inhibitors in triple-negative breast cancer cells. Sci Signal. 2013;6(287):ra66. [PubMed: 23921085]
30. Goyette MA, Duhamel S, Aubert L, Pelletier A, Savage P, Thibault MP, et al. The Receptor Tyrosine Kinase AXL Is Required at Multiple Steps of the Metastatic Cascade during HER2-Positive Breast Cancer Progression. Cell Rep. 2018;23(5):1476–90. [PubMed: 29719259]
31. Gjerdrum C, Tiron C, Hoiby T, Stefansson I, Haugen H, Sandal T, et al. Axl is an essential epithelial-to-mesenchymal transition-induced regulator of breast cancer metastasis and patient survival. Proc Natl Acad Sci U S A. 2010;107(3):1124–9. [PubMed: 20080645]
32. Shiozawa Y, Pedersen EA, Patel LR, Ziegler AM, Havens AM, Jung Y, et al. GAS6/AXL axis regulates prostate cancer invasion, proliferation, and survival in the bone marrow niche. Neoplasia. 2010;12(2):116–27. [PubMed: 20126470]
33. Loges S, Schmidt T, Tjwa M, van Geyte K, Lievens D, Lutgens E, et al. Malignant cells fuel tumor growth by educating infiltrating leukocytes to produce the mitogen Gas6. Blood. 2010;115(11): 2264–73. [PubMed: 19965679]
34. Lee GY, Kenny PA, Lee EH, Bissell MJ. Three-dimensional culture models of normal and malignant breast epithelial cells. Nat Methods. 2007;4(4):359–65. [PubMed: 17396127]
35. LaMarca HL, Visbal AP, Creighton CJ, Liu H, Zhang Y, Behbod F, et al. CCAAT/enhancer binding protein beta regulates stem cell activity and specifies luminal cell fate in the mammary gland. Stem Cells. 2010;28(3):535–44. [PubMed: 20054865]
36. Goruppi S, Chiaruttini C, Ruaro ME, Varnum B, Schneider C. Gas6 induces growth, beta-catenin stabilization, and T-cell factor transcriptional activation in contact-inhibited C57 mammary cells. Mol Cell Biol. 2001;21(3):902–15. [PubMed: 11154277]
37. Goruppi S, Ruaro E, Schneider C. Gas6, the ligand of Axl tyrosine kinase receptor, has mitogenic and survival activities for serum starved NIH3T3 fibroblasts. Oncogene. 1996;12(3):471–80. [PubMed: 8637702]
38. Paccez JD, Vasques GJ, Correa RG, Vasconcellos JF, Duncan K, Gu X, et al. The receptor tyrosine kinase Axl is an essential regulator of prostate cancer proliferation and tumor growth and represents a new therapeutic target. Oncogene. 2013;32(6):689–98. [PubMed: 22410775]
39. Asiedu MK, Beauchamp-Perez FD, Ingle JN, Behrens MD, Radisky DC, Knutson KL. AXL induces epithelial-to-mesenchymal transition and regulates the function of breast cancer stem cells. Oncogene. 2014;33(10):1316–24. [PubMed: 23474758]
40. Bohrer LR, Chuntova P, Bade LK, Beadnell TC, Leon RP, Brady NJ, et al. Activation of the FGFR-STAT3 pathway in breast cancer cells induces a hyaluronan-rich microenvironment that licenses tumor formation. Cancer Res. 2014;74(1):374–86. [PubMed: 24197137]
41. Behbod F, Gomes AM, Machado HL. Modeling Human Ductal Carcinoma In Situ in the Mouse. J Mammary Gland Biol Neoplasia. 2018.
42. Braunger J, Schleithoff L, Schulz AS, Kessler H, Lammers R, Ullrich A, et al. Intracellular signaling of the Ufo/Axl receptor tyrosine kinase is mediated mainly by a multi-substrate docking-site. Oncogene. 1997;14(22):2619–31. [PubMed: 9178760]
43. Shieh YS, Lai CY, Kao YR, Shiah SG, Chu YW, Lee HS, et al. Expression of axl in lung adenocarcinoma and correlation with tumor progression. Neoplasia. 2005;7(12):1058–64. [PubMed: 16354588]
44. Vouri M, Croucher DR, Kennedy SP, An Q, Pilkington GJ, Hafizi S. Axl-EGFR receptor tyrosine kinase hetero-interaction provides EGFR with access to pro-invasive signalling in cancer cells. Oncogenesis. 2016;5(10):e266. [PubMed: 27775700]
45. Buehler M, Tse B, Leboucq A, Jacob F, Caduff R, Fink D, et al. Meta-analysis of microarray data identifies GAS6 expression as an independent predictor of poor survival in ovarian cancer. Biomed Res Int. 2013;2013:238284. [PubMed: 23878800]

46. Wu X, Ma W, Zhou Q, Yan H, Lim ZF, Huang M, et al. AXL-GAS6 expression can predict for adverse prognosis in non-small cell lung cancer with brain metastases. J Cancer Res Clin Oncol. 2017;143(10):1947–57. [PubMed: 28551766]
47. Ben-Batalla I, Schultze A, Wroblewski M, Erdmann R, Heuser M, Waizenegger JS, et al. Axl, a prognostic and therapeutic target in acute myeloid leukemia mediates paracrine crosstalk of leukemia cells with bone marrow stroma. Blood. 2013;122(14):2443–52. [PubMed: 23982172]
48. Zucca LE, Morini Matushita MA, da Silva Oliveira RJ, Scapulatempo-Neto C, de Lima MA, Ribeiro GG, et al. Expression of tyrosine kinase receptor AXL is associated with worse outcome of metastatic renal cell carcinomas treated with sunitinib. Urol Oncol. 2018;36(1):11 e3–e21.
49. Bottai G, Raschioni C, Szekely B, Di Tommaso L, Szasz AM, Losurdo A, et al. AXL-associated tumor inflammation as a poor prognostic signature in chemotherapy-treated triple-negative breast cancer patients. NPJ Breast Cancer. 2016;2:16033. [PubMed: 28721387]
50. Mc Cormack O, Chung WY, Fitzpatrick P, Cooke F, Flynn B, Harrison M, et al. Growth arrest-specific gene 6 expression in human breast cancer. Br J Cancer. 2008;98(6):1141–6. [PubMed: 18283315]
51. Wu X, Liu X, Koul S, Lee CY, Zhang Z, Halmos B. AXL kinase as a novel target for cancer therapy. Oncotarget. 2014;5(20):9546–63. [PubMed: 25337673]
52. Kirane A, Ludwig KF, Sorrelle N, Haaland G, Sandal T, Ranaweera R, et al. Warfarin Blocks Gas6-Mediated Axl Activation Required for Pancreatic Cancer Epithelial Plasticity and Metastasis. Cancer Res. 2015;75(18):3699–705. [PubMed: 26206560]
53. Jerry DJ, Kuperwasser C, Downing SR, Pinkas J, He C, Dickinson E, et al. Delayed involution of the mammary epithelium in BALB/c-p53null mice. Oncogene. 1998;17(18):2305–12. [PubMed: 9811461]
54. Zhang X, Goncalves R, Mosser DM. The isolation and characterization of murine macrophages. Curr Protoc Immunol. 2008;Chapter 14:Unit 14 1.
55. Weischenfeldt J, Porse B. Bone Marrow-Derived Macrophages (BMM): Isolation and Applications. CSH Protoc. 2008;2008:pdb prot5080.

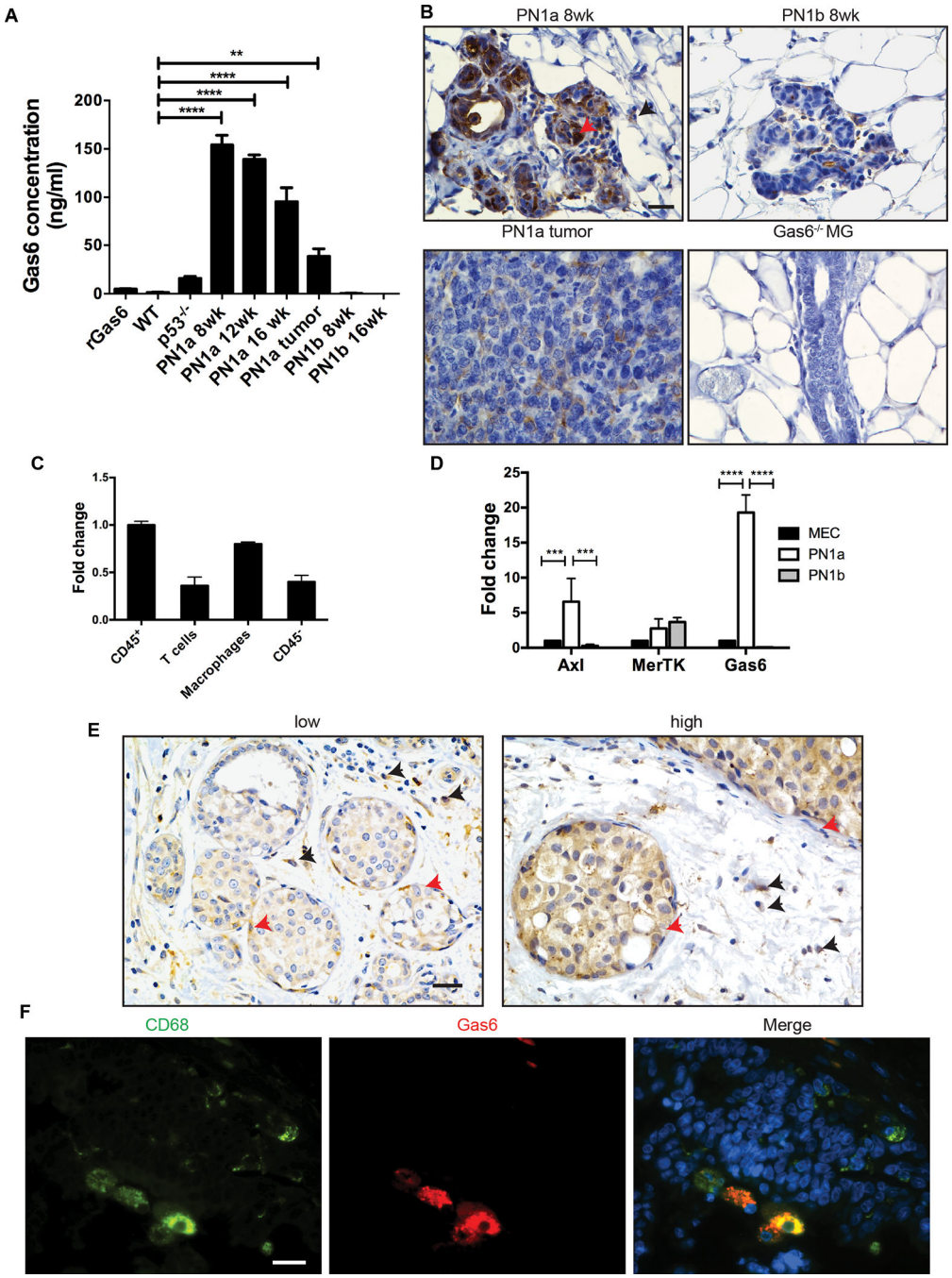

Figure 1: Gas6 and TAMR expression in pre-invasive lesions.

A) Mammary glands or tumors from wildtype, $p53^{-/-}$, or Balb/c mice containing PN1a or PN1b premalignant lesions were analyzed for Gas6 expression using ELISA. Recombinant Gas6 (rGas6) supplied by the manufacturer was used as positive control. Values shown (ng/ml of Gas6) are the mean and SEM from 3–6 independent experiments. ****p< 0.0001, **p< 0.01. **B)** Representative images of PN1a and PN1b tissues stained with a Gas6 antibody (n=3). Black arrowhead indicates Gas6 stromal staining and red arrowhead indicates Gas6 epithelial staining. $Gas6^{-/-}$ mammary glands (MG) were used as a negative

control. Scale bar= 20 μm. **C)** Cells were isolated from PN1a lesions at 8 weeks post-transplantation, FACS-sorted for $CD45^+$ ($CD45^+$), $CD45^+CD3^+CD11b^-$ (T cells), $CD45^+F4/80^+CD11b^+$ (macrophages) or $CD45^-$ cells, and qPCR for Gas6 was performed. Graph depicts 2^ddCT after normalizing to 18S, and fold changes were calculated by setting the highest value ($CD45^+$) equal to 1. Values shown are the mean and SD (n=3) from one representative experiment. **D)** LIN^- epithelial cells were FACS-sorted from normal mammary glands (MEC) or PN1a and PN1b lesions (8 weeks post-transplantation) and relative expression of Axl, MerTK and Gas6 was detected by qPCR. Graph depicts 2^ddCT after normalizing to 18S values shown are the mean and SD (n=3) from one representative experiment. Fold changes were calculated after setting MEC equal to 1. ***p< 0.001 and ****p< 0.0001 **E)** Representative images of human DCIS stained with a Gas6 antibody displaying low and high epithelial Gas6 expression. Red arrowhead indicates Gas6 epithelial staining, while black arrowhead shows Gas6 stromal staining. Scale bar = 10 μm. F) Representative images of immunofluorescence staining showing Gas6 (red) and CD68 (green) co-localization in human DCIS. Scale bar = 20 μm.

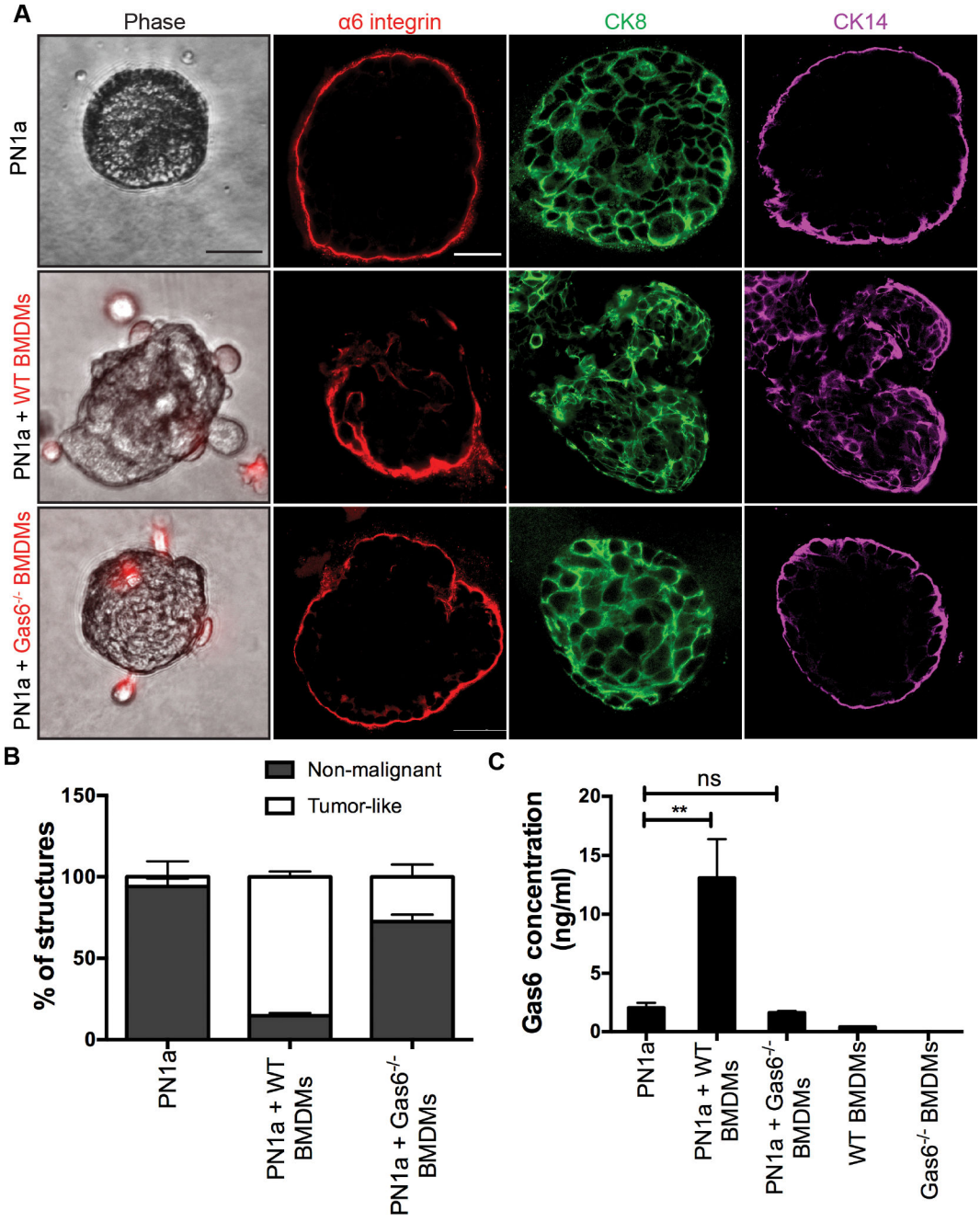

Figure 2: Macrophage-derived Gas6 induces a malignant phenotype *in vitro*.

Primary PN1a cells were cultured in Matrigel in the presence or absence of WT or Gas6$^{-/-}$ BMDMs (PKH26-labelled). **A)** Representative phase contrast images (BMDMs: red) and confocal images of structures immunostained with antibodies to α6 integrin (red), CK18 (green), and CK14 (purple). Scale bar=50 μm. **B)** Quantification of the number of tumor-like (disorganized, grape-like morphology) and non-malignant colonies. At least 30 structures per group were examined for each experiment from 3 independent experiments. Error bars represent SEM, ****p<0.0001. **C)** ELISA for Gas6 levels in supernatants collected after 10

days of co-culture (13 days total culture). Error bars represent SEM from 3 independent experiments (**p=0.0012).

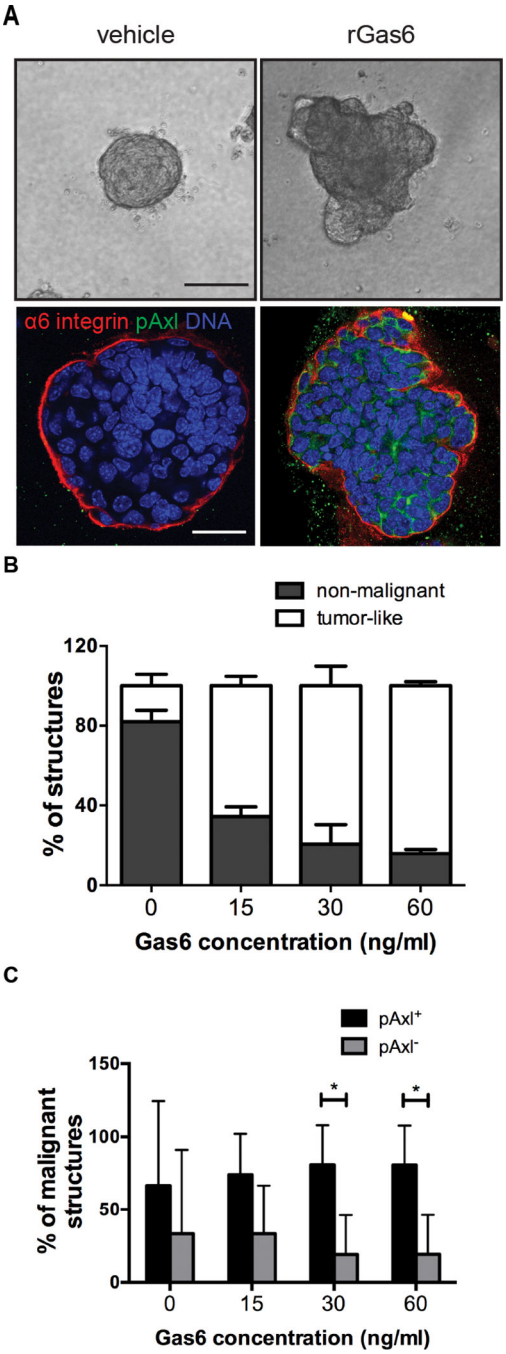

Figure 3: Gas6 treatment induces a malignant phenotype in PN1a cells.

PN1a cells were cultured in Matrigel in the presence or absence of various concentrations of rGas6 for 13 days. **A)** Representative phase contrast and confocal images depicting morphological changes induced by Gas6 treatment. Cells were stained with antibodies against pAxl (green) or α6 integrin and nuclei were detected with DAPI (blue). Scale bar=50 μm. **B)** Quantification of non-malignant and tumor-like structures resulting from treatment with various concentrations of rGas6 or vehicle (PBS) control. The number of non-malignant or tumor-like structures from a minimum of 30 colonies per group were counted

and expressed as a percent of total structures analyzed. Values shown are the mean and SEM from 3 independent experiments ($p<0.0001$). **C)** Graph depicts the presence or absence of pAxl staining within malignant structures after treatment with Gas6. Data are expressed as the percentage of total tumor-like structures (mean + SEM) from at least 30 colonies per group from 3 independent experiments (*$p< 0.05$).

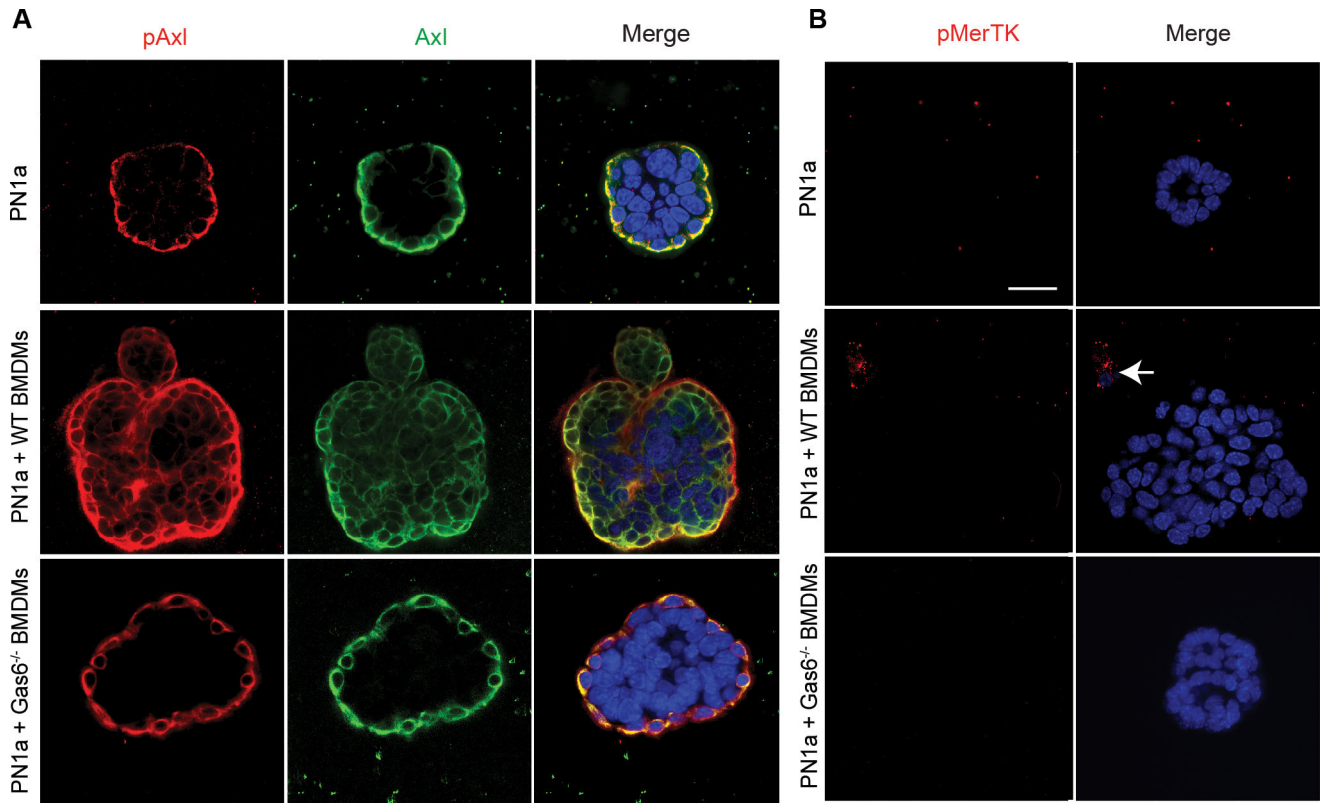

Figure 4: BMDMs induce Axl activation of pre-invasive cells.

PN1a cells were cultured in Matrigel in the presence or absence of WT or Gas6$^{-/-}$ BMDMs. Confocal images of structures stained with antibodies to **A)** pAxl (red), Axl (green) or **B)** pMerTK (red) are shown. Dapi staining was used to detect nuclei (blue). Arrow depicts pMerTK staining of a macrophage. Scale bar = 50 μm.

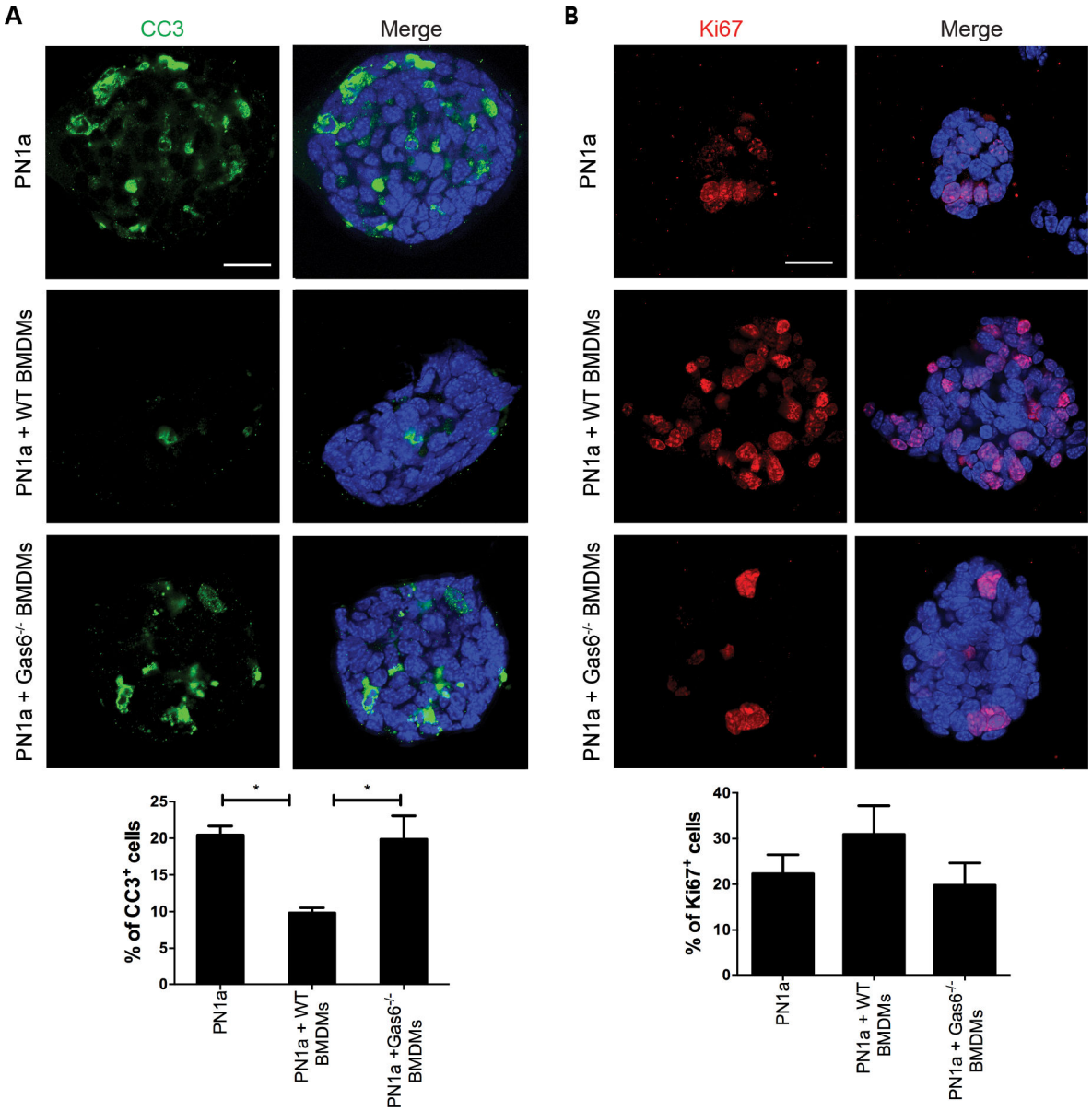

Figure 5: Macrophage-derived Gas6 increases premalignant mammary epithelial cell survival.

PN1a cells were cultured in Matrigel in the presence or absence of wildtype or Gas6$^{-/-}$ BMDMs for a total of 13 days. **A)** Confocal images of cells stained with an antibody to cleaved CC3 and the percentage of CC3^{+} cells was quantified. **B)** Confocal images showing Ki-67 staining and graph depicts the percentage of proliferating cells in each group. Values from both graphs represent the mean and SEM per field of view from 3 independent experiments (*p< 0.05). Scale bar = 50 μm.

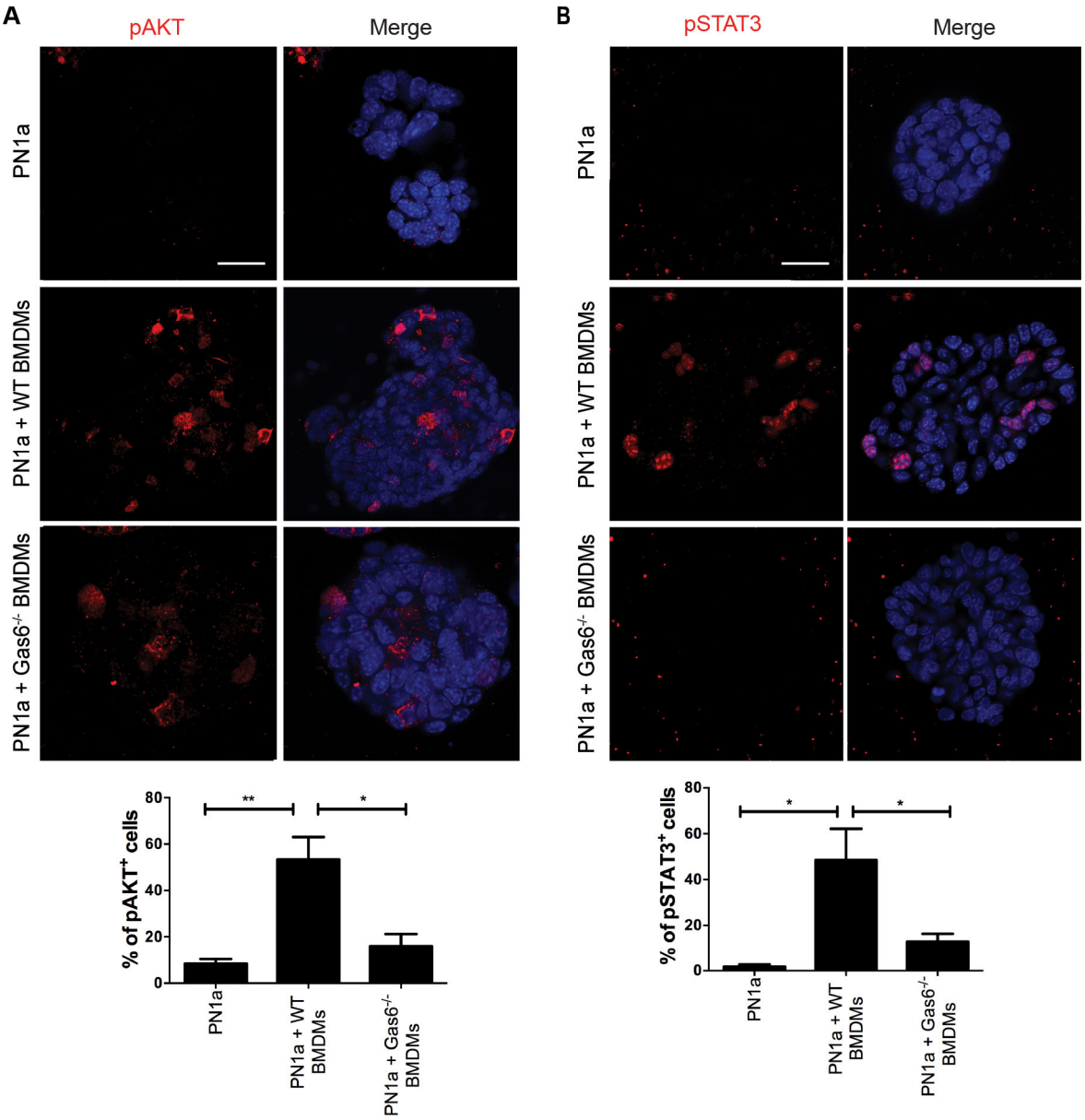

Figure 6: Macrophage-derived Gas6 activates AKT and STAT3 signaling in PN1a cells.

PN1a cells were cultured in Matrigel in the presence or absence of wildtype or Gas6$^{-/-}$ BMDMs for 13 days, and then they were fixed and stained with antibodies to pAKT and pSTAT3. **A)** Representative confocal images of pAKT staining and quantification of pAKT^{+} cells expressed as a percentage of total cells. **B)** Confocal images of pSTAT3 staining and quantification of pSTAT3^{+} cells expressed as a percentage of total cells. Nuclei were stained with DAPI (blue); scale bar = 50 μm. Values from both graphs represent the mean and SEM per field of view from 3 independent experiments (**p< 0.01 and *p< 0.05).

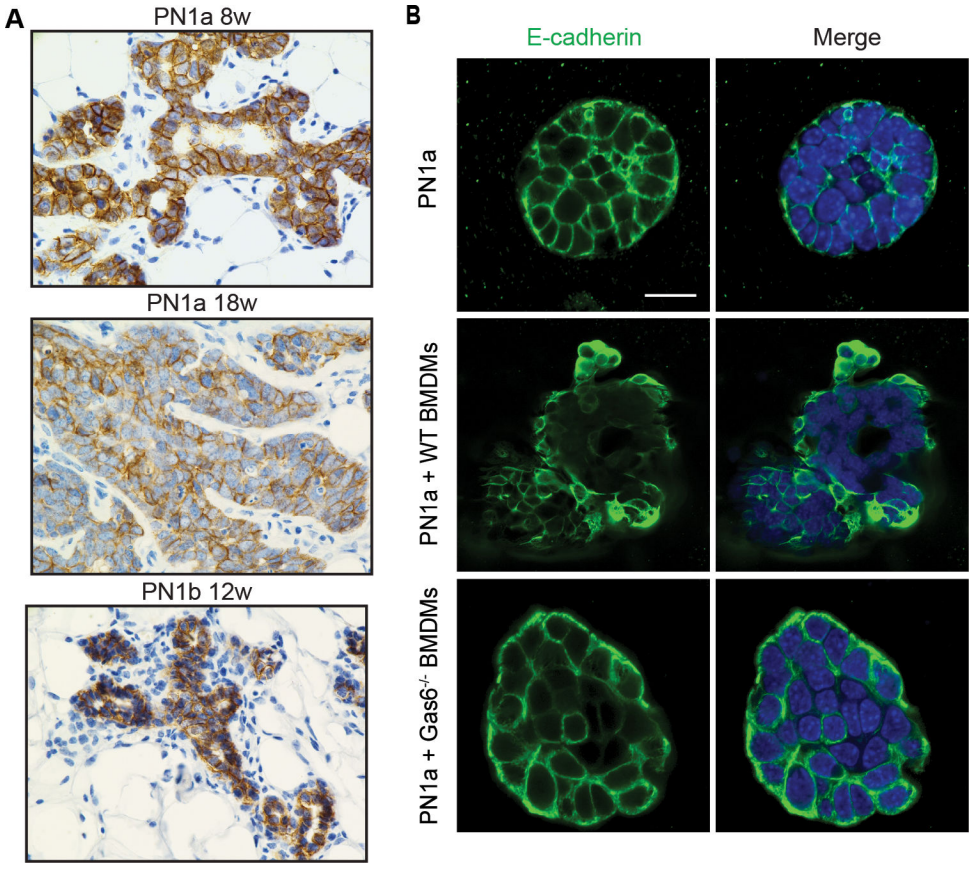

Figure 7: Macrophage-derived Gas6 promotes decreased E-cadherin expression.

A) Representative images of 8 week PN1a (n=4), 18 week PN1a (n=3) and 12 week PN1b (n=3) tissues stained with an E-cadherin antibody. Scale bar = 20 μm. **B)** PN1a cells were cultured in Matrigel in the presence or absence of wildtype or $Gas6^{-/-}$ BMDMs for 13 days, and then they were fixed and stained with an E-cadherin antibody (green) and nuclei were stained with DAPI (blue) (n=3). Representative confocal images of E-cadherin staining in PN1a cells are shown. Scale bar = 50 μm.

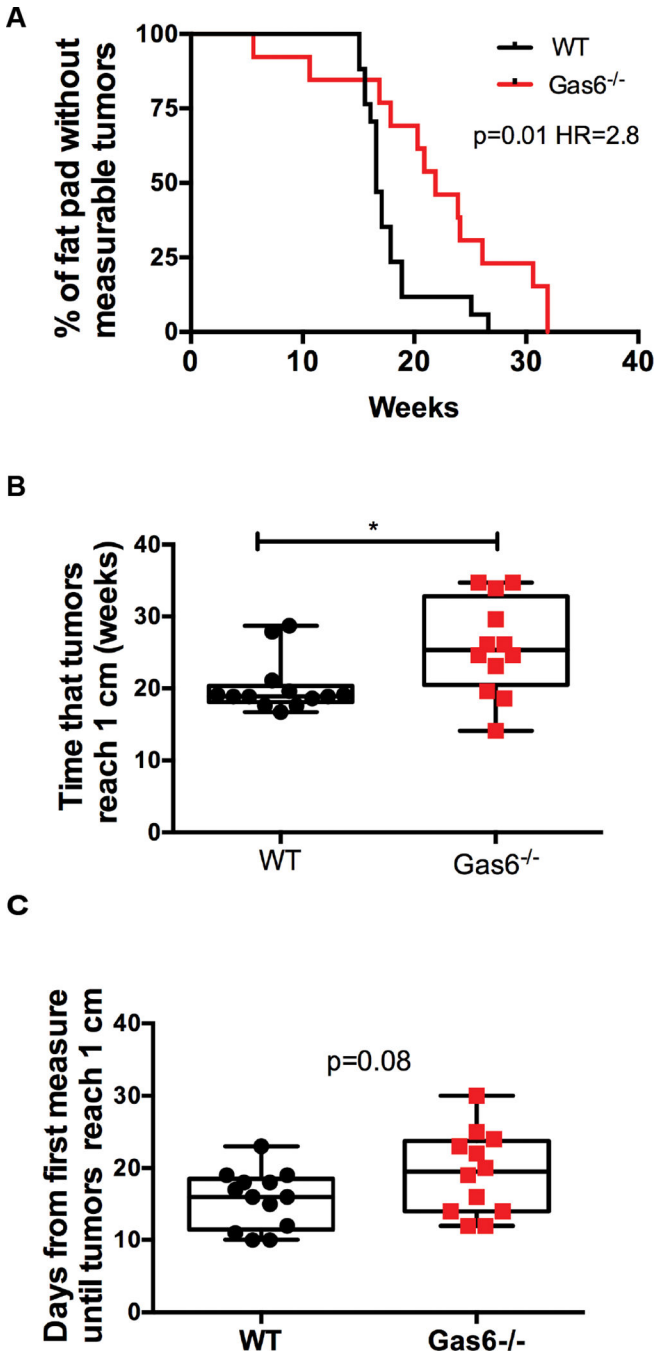

Figure 8: Stromal Gas6 deletion impairs the progression of PN1a lesions.

PN1a cells were transplanted into the cleared fat pads of wildype or Gas6$^{-/-}$ mice and allowed to progress to palpable tumors. Mice were euthanized when tumors reached 1 cm in diameter. **A)** Kaplan-Meier curve depicting the number of fat pads with palpable tumors at 0–35 weeks post-transplantation. 13 WT animals and 12 Gas6$^{-/-}$ animals were analyzed. The log rank test was used for statistical analysis (p=0.01). Hazard ratio (Mantel Haenszel)=2.8 with 95% CI=1.2 to 6.4. **B)** Box and whisker plot shows the number of weeks until tumors reached 1 cm in diameter. (*p< 0.05). **C)** Box and whisker plot depicting tumor

growth expressed as the number of days from when tumors are measurable (3 mm) until tumors reached 1 cm in diameter. (p=0.08).